Letter Vol. 48, No. 1 / 1 January 2023 / Optics Letters 175

Motion-resistant structured illumination microscopy based on principal component analysis

Jiaming Lyu,[1,†] Jiaming Qian,[2,3,4,†] Kailong Xu,[2,3,4] Yuxia Huang,[2,3,4] and Chao Zuo[2,3,4,*]

[1] Terahertz Technology Innovation Research Institute, University of Shanghai for Science and Technology, Shanghai 200093, China
[2] Smart Computational Imaging (SCI) Laboratory, Nanjing University of Science and Technology, Nanjing, Jiangsu Province 210094, China
[3] Smart Computational Imaging Research Institute (SCIRI), Nanjing University of Science and Technology, Nanjing, Jiangsu Province 210094, China
[4] Jiangsu Key Laboratory of Spectral Imaging & Intelligent Sense, Nanjing, Jiangsu Province 210094, China
*Corresponding author: zuochao@njust.edu.cn
† These authors contributed equally to this Letter.

Received 7 November 2022; revised 28 November 2022; accepted 28 November 2022; posted 1 December 2022; published 23 December 2022

Structured illumination microscopy (SIM) has become one of the most significant super-resolution techniques in bioscience for observing live-cell dynamics, thanks to fast full-field imaging and low photodamage. However, artifact-free SIM super-resolution reconstruction requires precise knowledge about variable environment-sensitive illumination parameters. Conventional algorithms typically, under the premise of known and reliable constant phase shifts, compensate for residual parameters, which will be easily broken by motion factors such as environment and medium perturbations, and sample offsets. In this Letter, we propose a robust motion-resistant SIM algorithm based on principal component analysis (mrPCA-SIM), which can efficiently compensate for nonuniform pixel shifts and phase errors in each raw illumination image. Experiments demonstrate that mrPCA-SIM achieves more robust imaging quality in complex, unstable conditions compared with conventional methods, promising a more compatible and flexible imaging tool for live cells.

https://doi.org/10.1364/OL.480330

In the past few decades, super-resolution techniques have bypassed the Abbe diffraction limit to visualize biomolecules at the nanoscale to single-molecule level, and have developed into a powerful tool for life science research [1]. Benefiting from the advantages of fast wide-field imaging, low photodamage, and the nonspecific requirement for fluorescent molecules, structured illumination microscopy (SIM) stands out from numerous super-resolution techniques, especially for real-time long-term dynamic observation of live cells [2–4].

Typically, SIM carries the high-frequency information originally exceeding the system cutoff frequency to the detection passband through spatial structured illumination modulation, thus doubling the lateral resolution [5]. To achieve high-quality image reconstruction, accurate estimation of illumination parameters, such as initial phase, is inevitably required, and minor parameter errors can cause severe reconstruction artifacts [6]. These illumination parameters are particularly sensitive to variable experimental environments, so unless imaging conditions are strictly maintained stable, *a posteriori* parameter extraction has to be performed per reconstruction for dynamic observation of live cells [7]. Conventional parameter estimation methods, such as the iterative cross-correlation (COR) approach, usually perform an initial spectrum separation with a known constant phase shift for each illumination orientation, and on this basis compensate for residual parameters [8]. However, in complex operating scenarios, environmental and media perturbations, artificial interference with experimental interactions, etc., can lead to frame-wise motion of the sample and illumination, which breaks the basic assumptions of conventional algorithms for uniform phase shifts and thus cause severe imaging artifacts [9,10]. Although motion-induced errors were attempted to be compensated, accuracy and efficiency were still limited [11]. Recently, we have proposed an environment-robust SIM algorithm based on principal component analysis (PCA-SIM), which applies PCA to remove illumination-independent disturbances and achieves precise parameter estimation (with much higher accuracy and efficiency than COR) in complex experimental conditions [12]. However, PCA-SIM remains as susceptible to motion factors as other conventional methods. In this Letter, we propose a robust motion-resistant SIM algorithm based on PCA (mrPCA-SIM). By efficiently compensating the motion-induced pixel offsets and phase errors for each original observation, the SIM super-resolution quality under complicated, unstable conditions is significantly enhanced.

The original structured illumination images D_n ($n = 1, 2, 3$) in motion with set constant phase shift φ in a certain illumination orientation can be represented as [Fig. 1(a)]

$$D_n(\mathbf{r}) = \{S(\mathbf{r}+\mathbf{r}_n)[1 + m\cos(2\pi\mathbf{k}_{ex}\mathbf{r} + (n-1)\varphi + \varphi_n)]\} \otimes P(\mathbf{r}), \quad (1)$$

where $\mathbf{r}$ is the image coordinate, S represents the sample information, $\mathbf{r}_n$ and φ_n denote the motion-induced pixel offset and phase error (here take the first frame as the reference and let $\mathbf{r}_n = 0$; note that the illumination shift due to dithering can be converted to phase error), P is the point spread function, $\otimes$ is the convolution operation, and $\mathbf{k}_{ex}$ and m are the wave vector

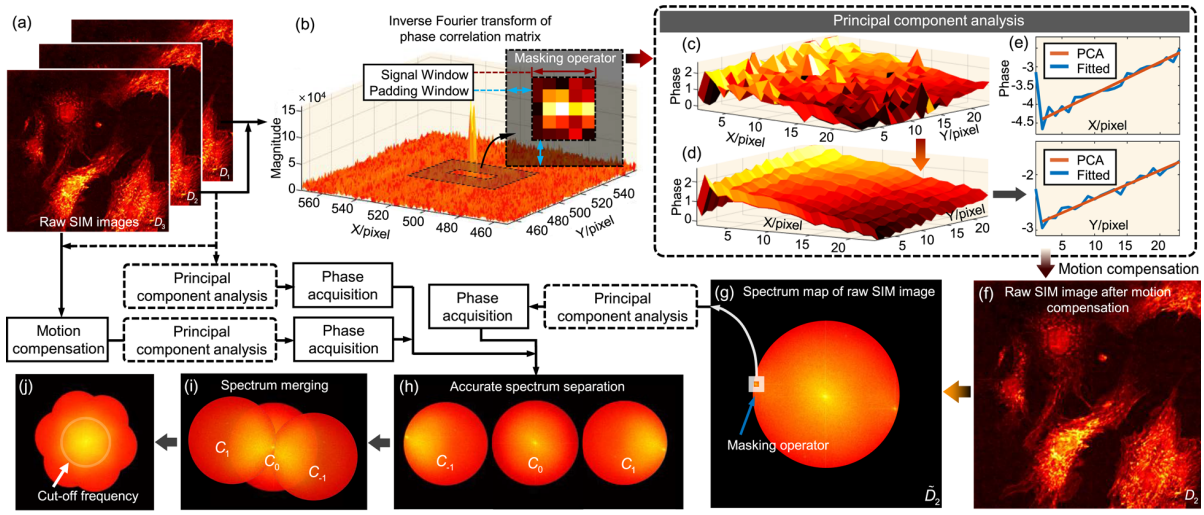

Fig. 1. Flow chart of mrPCA-SIM. (a) Raw SIM image in a certain illumination orientation in motion conditions. (b) Inverse Fourier transform of phase correlation matrix ψ between $\tilde{D}_1$ and $\tilde{D}_2$. (c) Phase distribution of ψ extracted by the masking operator. (d) Principal components of (c). (e) Least-squares fitting of the dominant singular vectors. (f) D_2 after offset compensation. (g) Spectrum of (f). (h),(i) Spectra that are precisely separated and merged. (j) Merged spectrum of three illumination orientations.

and modulation depth of the illumination pattern, respectively. Their spectra can be obtained by Fourier transform:

$$\tilde{D}_n(\mathbf{k}) = \left[\frac{m}{2} O(\mathbf{k}) \tilde{S}_{\pm 1}(\mathbf{k} \mp \mathbf{k}_{ex}) e^{\pm j[(n-1)\varphi + \varphi_n]} + O(\mathbf{k}) \tilde{S}_0(\mathbf{k})\right] e^{j\mathbf{k}\mathbf{r}_n}, \tag{2}$$

where $\mathbf{k}$ represents the frequency coordinate, $\sim$ denotes the Fourier transform of the original object, subscripts 0 and ± 1 are the orders of the separated spectra, and O represents the optical transfer function (OTF). In $\tilde{D}_n$, the zeroth-order spectrum (C_0) represents the diffraction-limited wide-field information and the first-order spectra ($C_{\pm 1}$) are the super-resolution data to be demodulated. It can be seen from Eq. (2) that the motion causes frame-specific phase errors in the frequency domain, which will seriously affect accurate spectrum separation and merging, resulting in imaging artifacts. Among the motion interference, the pixel offset $e^{j\mathbf{k}\mathbf{r}_n}$ is the Fourier transform of a delta function, whose peak just reflects the offset. Since the zeroth-order spectrum is only modulated by $e^{j\mathbf{k}\mathbf{r}_n}$, it can be directly extracted by calculating the normalized cross power spectrum between the zeroth-order spectrum of the shifted map and that of the reference ($\tilde{D}_1$):

$$\psi(\mathbf{k}) = \frac{[\tilde{D}_n(\mathbf{k})][\tilde{D}_1(\mathbf{k})]^* \mathrm{Han}(\mathbf{k})}{|[\tilde{D}_1(\mathbf{k})][\tilde{D}_1(\mathbf{k})]^*|} \approx e^{j\mathbf{k}\mathbf{r}_n}, \tag{3}$$

where ψ represents the phase correlation matrix, $*$ denotes the complex conjugate, and Han is a Hanning filter with a radius of the peak distance between the zeroth- and first-order spectra, which is used to attenuate the non-zeroth-order spectra that were originally fading in the central image region. However, the offset of non-integer pixels will spread the spectrum peak of the inverse Fourier transform of ψ toward the neighborhood, which, together with the interference factors such as noise and spectral residuals of other orders, will lead to offset estimation error [Fig. 1(b)]. Actually, the task of extracting $e^{j\mathbf{k}\mathbf{r}_n}$ here is similar to recovering the illumination phasor matrix in PCA-SIM (see Note S1 in Ref. [13] for details), which inspires us to state that $e^{j\mathbf{k}\mathbf{r}_n}$ is essentially a rank-one matrix decomposable into $\rho_x \rho_y^H$ (where $\rho_x = e^{j\mathbf{k}_x \mathbf{r}_x}$, $\rho_y = e^{-j\mathbf{k}_y \mathbf{r}_y}$, subscripts x and y represent the components along the horizontal and vertical directions, and the superscript H indicates the complex-conjugate transpose) that contains one principal component describing the single best subspace in the least squares sense. To extract this principal component from ψ, which is subject to interference that leads to high dimensionality, we apply PCA based on singular value decomposition (SVD) to perform data dimensionality reduction on ψ. As shown in Figs. 1(c) and 1(d), the phase distribution of ψ after PCA is significantly closer to its ideal form ($\mathbf{k}_x \mathbf{r}_n$). The offset $\mathbf{r}_n$ of subpixel accuracy can then be accessed by least squares fitting of the left and right dominant singular vectors and taking their slopes [Fig. 1(e)]. In addition, considering that the discrete inverse Fourier transform of ψ is an approximate energy-concentrated two-dimensional (2D) Dirichlet function, we use a double-window masking operator to further improve the accuracy of pixel offset estimation while reducing the amount of data involved in PCA and improving the processing efficiency [12]. The introduced masking operator consists of a signal window and a padding window, where the former is designed to extract the concentrated energy with high signal-to-noise ratio (SNR) and truncate the noise, and the latter is for interpolation of the Fourier transform of the signal window to increase the fitting accuracy [Fig. 1(b)].

After compensating for $\mathbf{r}_n$, it is required to estimate the motion-induced phase $[\varphi_n' = (n-1)\varphi + \varphi_n]$ for each observation rather than just a fixed initial phase as in the conventional scheme [Figs. 1(f) and 1(g)]. In the frequency domain, the phase behaves as the e-exponential term of first-order spectra. Taking the +1-order spectrum as an example, its inverse Fourier transform of the sample part can be expressed as $S_1(\mathbf{r}) e^{j(\mathbf{k}_{ex}\mathbf{r} + \varphi_n')}$, revealing that extracting φ_n' from a version suffering from various disturbances (e.g., noise, attenuation of OTF, cross talk from other spectral orders, etc.) is essentially consistent with the above task of extracting $\mathbf{r}_n$ from ψ. Therefore, we directly apply PCA combined with the masking operator to solve for the precise phase of each frame; specifically, extract the energy-concentrated, dominant first-order spectrum of $\tilde{D}_n$ using the masking operator, then acquire the principal component of its inverse Fourier transform by PCA, and finally take

the phase at $\mathbf{r} = \mathbf{0}$. Through the acquired frame-specific phases, the illumination images after offset compensation can be combined linearly to accurately separate and reorganize the spectra [Figs. 1(h) and 1(i)]. Repeating the above steps in another two illumination orientations eventually achieves an isotropic lateral resolution enhancement [Fig. 1(j)] (see Note S2 in Ref. [13] for details).

Some simulations were conducted to verify the effectiveness of mrPCA-SIM. We artificially added nonuniform phase-shifted illumination patterns to a high-resolution cell image to generate the simulation data, while introducing frame-wise non-integer pixel offsets. As mentioned before, the motion-induced errors lead to spectrum separation failures in the conventional SIM method (here we use PCA-SIM, a state-of-the-art parameter estimation technique) without considering motion compensation, where the separated spectrum components carry significant cross talk from other orders [white circled region in Fig. 2(b)]. In contrast, mrPCA-SIM achieves accurate spectrum separation and merging [Figs. 2(c)–2(e)], and reconstructs an artifact-free super-resolution image comparable to the ground truth [Figs. 2(f)–2(i)]. For optimal accuracy and efficiency, the dual-window sizes of the masking operator are 7×7 and 23×23

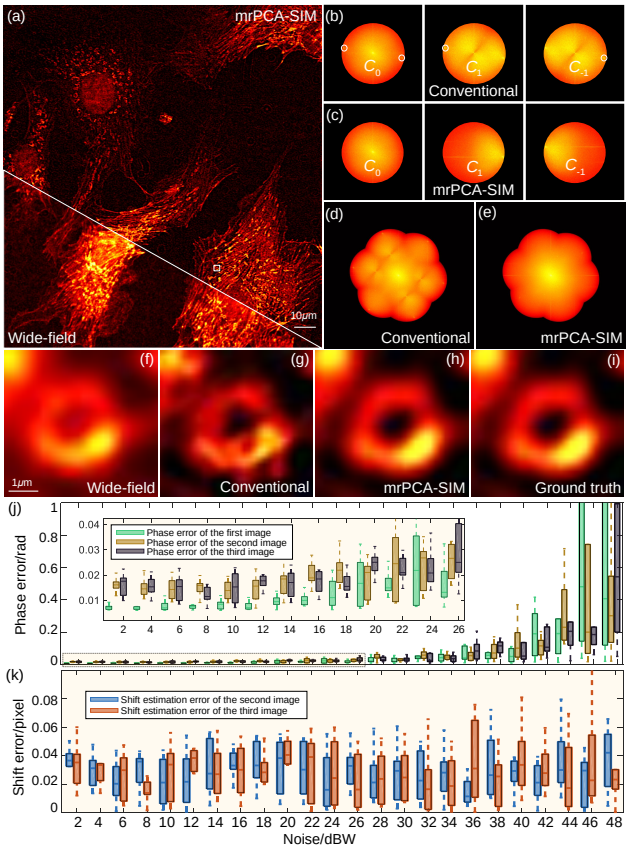

Fig. 2. Simulation results of mrPCA-SIM. (a) Wide-field image and super-resolution image obtained by mrPCA-SIM. (b),(c) Spectra separated by conventional method and mrPCA-SIM. (d),(e) Spectra merged by conventional method and mrPCA-SIM. (f)–(i) Magnified wide-field image, result obtained by conventional method, that obtained by mrPCA-SIM, and the label from boxed region in (a). (j),(k) Phase and offset estimation errors of mrPCA-SIM in different SNRs. Simulations were repeated ten times independently with similar results.

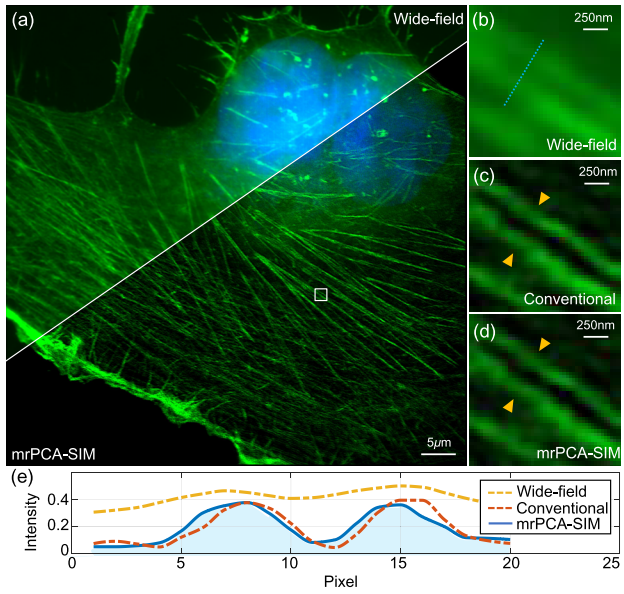

Fig. 3. Super-resolution results for COS-7 cells in stable environments. (a) Wide-field and super-resolution images obtained by mrPCA-SIM. (b)–(d) Magnified wide-field and super-resolution images of actin from boxed region in (a) obtained by different methods. (e) Intensity profiles along blue line in (b).

[12]. The quantified data at different SNRs indicate that mrPCA-SIM yields a phase accuracy of less than 0.02 rad and offset accuracy of less than 0.05 pixels at regular SNRs (note that the relatively large phase errors of the second and third images are caused by offset errors), and exhibits superior noise immunity at low SNRs.

Next, we constructed a SIM system (Fig. S1 in Ref. [13]) and measured some fixed cells to further validate the advancement of mrPCA-SIM. Figure 3 illustrates the super-resolution results for a COS-7 (CV-1 in Origin Simian-7) sample in stable environments. Because of accurate phase estimation, mrPCA-SIM acquires a visually similar result to that acquired by the conventional SIM method with known constant phase shift. Intensity profile analysis of the amplified actin indicates that mrPCA-SIM under steady imaging conditions enables the same performance of resolution enhancement as the conventional method [Figs. 3(b)–3(d)]. We then set nonuniform phase-shifted structured illumination and slightly moved the microscope carrier during imaging to produce motion scenarios. In such conditions, mrPCA-SIM still maintains high imaging quality and resolves fine actin structures, whereas the conventional method suffers from significant reconstruction artifacts (Fig. 4).

One of the main applications of mrPCA-SIM is to cope with environmental fluctuations caused by motion factors in real-time live-cell observations. To verify this, we applied mrPCA-SIM to perform real-time super-resolution imaging of live COS-7 mitochondria under motion scenarios. Figures 5(a)–5(c) present the super-resolution results for COS-7 mitochondria at a certain time for both the conventional method and mrPCA-SIM. It can be seen that the conventional method is vulnerable to motion and consequently severe reconstruction artifacts appear (note that the dynamics of cells themselves cause only minor and negligible artifacts), while these artifacts are effectively suppressed by mrPCA-SIM due to accurate pixel offset and phase error correlation, even at low SNRs caused by severe

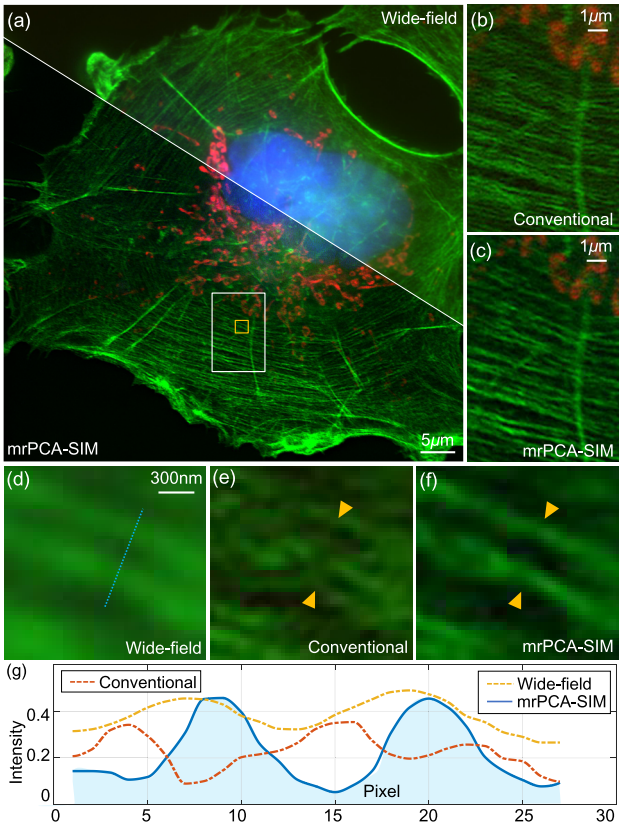

Fig. 4. Super-resolution results for COS-7 cells in motion environments. (a) Wide-field and super-resolution images obtained by mrPCA-SIM. (b),(c) Magnified super-resolution images from white boxed region in (a) obtained by different methods. (d)–(f) Magnified results for actin from yellow boxed region in (a). (g) Intensity profiles along blue line in (d).

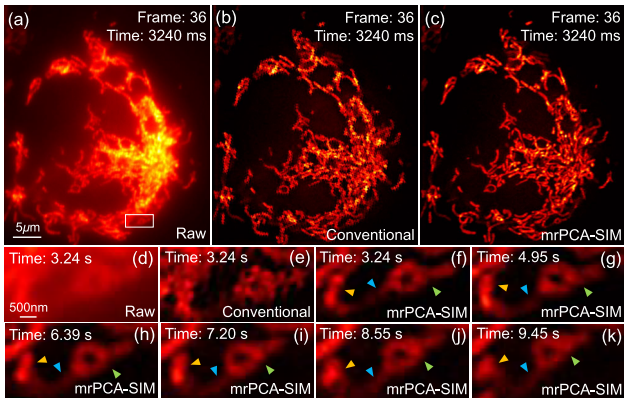

Fig. 5. Super-resolution results for live COS-7 mitochondria at different moments. (a)–(c) Wide-field and super-resolution images obtained by mrPCA-SIM. (d)–(f) Magnified wide-field and super-resolution images from boxed region in (a) obtained by different methods. (g)–(k) Magnified super-resolution images from boxed region in (a) obtained by mrPCA-SIM.

out-of-focus sample [Figs. 5(d)–5(f)]. In terms of running speed, the time cost of C++-based software developed on a Dell XPS 8930 computer is about 40 ms. Robustness to complex environments allows mrPCA-SIM to reconstruct dynamic mitochondrial tubule events with high quality (complete dynamic results are provided in Visualization 1). As shown in Figs. 5(f)–5(k), the right mitochondrion extends the elongated mitochondrial tubule toward the left one and drags it to deformation, and these phenomena are valuable for studying the formation of mitochondrial networks (see Note S3 in Ref. [13] for further simulation and experiment details).

In summary, efficient processing performance and robustness to complicated scenarios make mrPCA-SIM a promising tool for real-time observation of live cells that is more flexible, more cost-effective for maintaining stable environments, and more interactive. Although mrPCA-SIM can deal with motion-induced lateral shifts and phase errors, the disturbances caused by unstable environments during practical imaging are much more than that, e.g., the transient artifacts at 13 s in Visualization 1 are caused by out-of-focus sample due to axial fluctuations. Since SIM is essentially a multi-frame imaging approach, minimizing the number of structured illumination images required per reconstruction can further alleviate impacts of unstable environments under dynamic imaging conditions, which is our future focus.

Funding. National Natural Science Foundation of China (61905115, 62105151, 62175109, U21B2033); National Major Scientific Instrument Development Project (62227818); Leading Technology of Jiangsu Basic Research Plan (BK20192003); Youth Foundation of Jiangsu Province (BK20190445, BK20210338); Biomedical Competition Foundation of Jiangsu Province (BE2022847); Key National Industrial Technology Cooperation Foundation of Jiangsu Province (BZ2022039); Fundamental Research Funds for the Central Universities (30920032101); Open Research Fund of Jiangsu Key Laboratory of Spectral Imaging & Intelligent Sense (JSGP202105, JSGP202201).

Disclosures. The authors declare no conflicts of interest.

Data availability. Data underlying the results presented in this paper are not publicly available at this time but may be obtained from the authors upon reasonable request.

REFERENCES

1. Y. Fan, J. Li, L. Lu, J. Sun, Y. Hu, J. Zhang, Z. Li, Q. Shen, B. Wang, R. Zhang, Q. Chen, and C. Zuo, PhotoniX **2**, 19 (2021).
2. M. G. Gustafsson, J. Microsc. **198**, 82 (2000).
3. J. Qian, Y. Cao, K. Xu, Y. Bi, W. Xia, Q. Chen, and C. Zuo, Appl. Phys. Lett. **121**, 153701 (2022).
4. Z. Wang, T. Zhao, H. Hao, Y. Cai, K. Feng, X. Yun, Y. Liang, S. Wang, Y. Sun, P. R. Bianco, K. Oh, and M. Lei, Adv. Photonics **4**, 026003 (2022).
5. G. Wen, S. Li, L. Wang, X. Chen, Z. Sun, Y. Liang, X. Jin, Y. Xing, Y. Jiu, Y. Tang, and H. Li, Light: Sci. Appl. **10**, 70 (2021).
6. X. Huang, J. Fan, L. Li, H. Liu, R. Wu, Y. Wu, L. Wei, H. Mao, A. Lal, P. Xi, L. Tang, Y. Zhang, Y. Liu, S. Tan, and L. Chen, Nat. Biotechnol. **36**, 451 (2018).
7. K. Wicker, Opt. Express **21**, 24692 (2013).
8. M. G. Gustafsson, L. Shao, P. M. Carlton, C. R. Wang, I. N. Golubovskaya, W. Z. Cande, D. A. Agard, and J. W. Sedat, Biophys. J. **94**, 4957 (2008).
9. R. Förster, W. Kai, W. Müller, A. Jost, and R. Heintzmann, Opt. Express **24**, 22121 (2016).
10. R. Förster, W. Müller, R. Richter, and R. Heintzmann, Opt. Express **26**, 20680 (2018).
11. R. Turcotte, Y. Liang, M. Tanimoto, Q. Zhang, Z. Li, M. Koyama, E. Betzig, and N. Ji, Proc. Natl. Acad. Sci. **116**, 9586 (2019).
12. J. Qian, Y. Cao, Y. Bi, H. Wu, Y. Liu, Q. Chen, and C. Zuo, eLight **2**, 70 (2022).
13. J. Lyu and J. Qian, "Supplementary material for mrPCA-SIM," https://doi.org/10.6084/m9.figshare.21628484.v1 Accessed November 25, 2022.